

Cite this: *Nanoscale*, 2015, 7, 9779

Spatial modulation spectroscopy for imaging and quantitative analysis of single dye-doped organic nanoparticles inside cells†

Mary Sajini Devadas,‡ Tuphan Devkota,‡ Samit Guha, Scott K. Shaw, Bradley D. Smith and Gregory V. Hartland*

Imaging of non-fluorescent nanoparticles in complex biological environments, such as the cell cytosol, is a challenging problem. For metal nanoparticles, Rayleigh scattering methods can be used, but for organic nanoparticles, such as dye-doped polymer beads or lipid nanoparticles, light scattering does not provide good contrast. In this paper, spatial modulation spectroscopy (SMS) is used to image single organic nanoparticles doped with non-fluorescent, near-IR croconaine dye. SMS is a quantitative imaging technique that yields the absolute extinction cross-section of the nanoparticles, which can be used to determine the number of dye molecules per particle. SMS images were recorded for particles within EMT-6 breast cancer cells. The measurements allowed mapping of the nanoparticle location and the amount of dye in a single cell. The results demonstrate how SMS can facilitate efforts to optimize dye-doped nanoparticles for effective photothermal therapy of cancer.

Received 12th March 2015,

Accepted 2nd May 2015

DOI: 10.1039/c5nr01614b

www.rsc.org/nanoscale

Introduction

Cell imaging at high spatial resolution is important for understanding biological function,^{1–4} and the development of sensitive, high-resolution imaging techniques is at the forefront of biomedical research.^{5–12} Typically imaging in cells is done either using fluorescent tags^{1–4} or with metal nanoparticles that efficiently scatter light.^{13–16} However, techniques based on fluorescence or light scattering do not work well in the near-IR, which is an important spectral region for *in vivo* experiments.^{17–19} This is because of the poor sensitivity of CCD and PMT detectors in the near-IR region, and the typical low quantum yields of near-IR emitting dyes.^{20,21} In contrast, imaging techniques that detect nanoparticles through their absorption or extinction, such as photothermal heterodyne imaging (PHI)^{22–26} and spatial modulation spectroscopy (SMS),^{27,28} do not rely on high sensitivity detectors. These techniques can be readily used to study nanomaterials that absorb in the near-IR region.^{29–32} In addition to improved near-IR sen-

sitivity, absorption measurements perform better for small nanoscale objects compared to scattering measurements because of the way scattering scales with volume.^{22,33} Of these two techniques, PHI is the more sensitive.²⁵ However, SMS has an advantage in that it directly provides quantitative information about the extinction cross-section of the nanoparticle. For metal nanoparticles this allows the size of the particle to be determined, which is very useful for spectroscopic studies.^{34,35}

A class of near-IR absorbing materials that has recently gained considerable attention for photothermal therapy applications are dye-doped hybrid lipid-polymer nanoparticles (LPNPs).^{36–42} These materials comprise a polymeric core coated with a layer of phospholipid, with a suitable organic dye incorporated into the hydrophobic core. In our experiments the core is doped with a croconaine dye, and we have shown that croconaine-doped LPNPs have a similar absorption cross-section in the near-IR to the gold nanostructures that are typically used in photothermal therapy.^{42–45} Their intense near-IR absorption, low fluorescence quantum yield, and resistance to photobleaching combine to make croconaine dyes a promising system for efficient photothermal treatment of cancer cells.^{46,47} An important step in advancing the use of dye-doped organic nanoparticles for photothermal therapy is to optimize the dye loading and intracellular delivery. However, the lack of fluorescence from the dyes makes it very difficult to image these particles in biological environments. A possible solution to this problem is to co-dope the particles

Department of Chemistry and Biochemistry, University of Notre Dame, Notre Dame, IN 46556-5670, USA. E-mail: ghartlan@nd.edu

†Electronic supplementary information (ESI) available: TEM imaging, calibration experiments for the SMS instrument with gold nanoparticles, SMS images of dye doped polymer beads from a commercial source, evidence for endosome uptake, and additional SMS images of dye-doped LPNPs in EMT-6 cells, and spectra of SRfluor680/croconaine doped lipid-polymer nanoparticles. See DOI: 10.1039/C5NR01614B

‡These students contributed equally to this work.

with two different dyes: one to supply the photothermal effect and another that allows fluorescence imaging. However, this type of dual modality is difficult to achieve for systems designed for *in vivo* imaging, as emission is typically quenched for a deep-red fluorescent dye molecule in close proximity to a non-fluorescent near-IR absorbing partner.

In this paper SMS has been used to determine the extinction cross-sections of individual croconaine-doped LPNPs, which allows us to estimate the number of dye molecules inside each particle – a parameter that is difficult to determine using conventional techniques. This approach is similar to that used in the recent PHI studies of dye nanoparticles described by Gaiduk and co-workers.⁴⁸ However, our measurements do not rely on the use of an internal standard to calibrate the signal (*e.g.*, 20 nm gold particles were used in ref. 48). SMS was also used to image dye-doped LPNPs that were taken up by living cancer cells. The images reveal the intracellular location of the particles and the number of dye molecules incorporated into the cells.^{49,50} The results establish SMS as a promising technique for direct and quantitative characterization of non-fluorescent organic nanoparticles inside cells.

Results and discussion

SMS images of croconaine-doped LPNPs, spin coated onto a microscope coverslip, are presented in Fig. 1. In SMS the sample is spatially modulated by a few hundred nanometers.²⁷ This causes a modulation in the transmitted or reflected power of a focused laser beam when it is scanned over a particle, which is monitored by a lock-in amplifier. The signal has a derivative-type lineshape for detection at the fundamental of the modulation frequency,²⁷ which is clearly seen in Fig. 1. Fig. 1(A) shows an image recorded at 785 nm, which is close to the absorption maximum of the near-IR dye, and Fig. 1(B) shows an image of the same region of the sample recorded at 637 nm. As expected the amplitude of the SMS signal is significantly reduced at 637 nm, as the croconaine dye has virtually no absorption at this wavelength (see Fig. 4 below). This also shows that isolated croconaine-doped LPNPs do not significantly scatter light in these measurements, as scattering should be more pronounced at 637 nm than at 785 nm. This is expected as TEM images show that the LPNPs are smaller than several hundred nanometers (see the ESI†), and therefore should not scatter light strongly.

We also studied LPNPs that were doped with a mixture of near-IR croconaine dye and red SRfluor680 dye (which absorbs at 640 nm). The normally fluorescent SRfluor680 dye was strongly quenched by energy transfer to the nearby co-encapsulated croconaine. This illustrates the difficulty of creating co-doped dye organic nanoparticle systems that have photothermal and fluorescence modalities. The absence of any SRfluor680 fluorescence increase in the samples throughout the experiments is also good evidence that the particles did not leak dye. Fig. 1(C) and (D) show SMS images of these binary dye-doped LPNPs recorded at 785 nm and 637 nm,

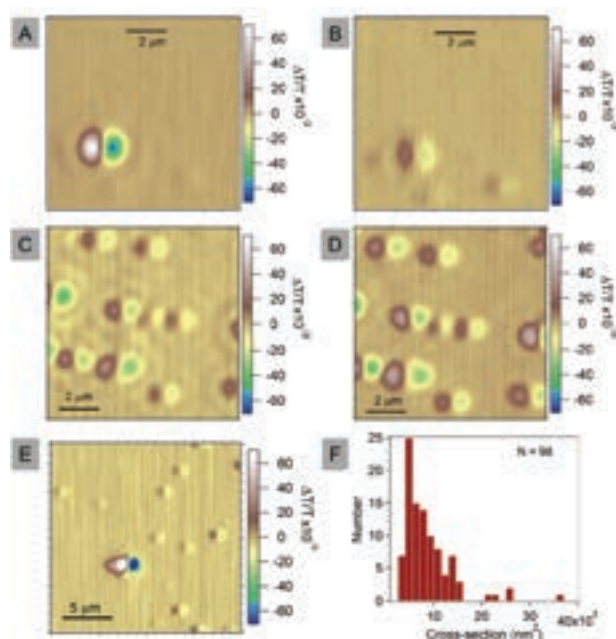


Fig. 1 (A) Contour plot of 1f SMS data recorded at 785 nm for the croconaine-doped LPNPs. (B) The same area as in panel (A) recorded at 637 nm. (C) 1f SMS image of LPNPs doped with croconaine and SRfluor680 dyes recorded at 785 nm. (D) The same area as panel (C) recorded at 637 nm. (E) A larger area 1f image recorded at 785 nm for the croconaine only doped LPNPs showing a distribution of signal strengths (different area than panel (A)). The strong signal near the middle of the image is probably due to several particles aggregated together. (F) Histogram of the extinction cross-section per particle determined from the SMS measurements.

respectively. In this case the system has significant absorption at both wavelengths, and the particles show up with approximately the same signal level in both images (absorption spectra of the SRfluor680 dye, and the SRfluor680 and croconaine doped LPNPs are given in the ESI†). These images form a control experiment for the measurements in Fig. 1(A) and (B), and also show that it is possible to identify different types of dye doped nanoparticles by performing dual wavelength measurements.

Analysis of the SMS images allows us to determine the extinction cross-sections of the particles. Specifically, assuming a Gaussian beam shape at the sample, the signal in the SMS experiments (the relative change in power of the detected laser beam) for a nanoparticle positioned at $(x,y) = (0,0)$ is given by^{27,28,51}

$$\frac{\Delta P}{P} = \frac{8}{\pi} \frac{\delta \sigma_p}{w_0^4} x e^{-2(x^2+y^2)/w_0^2} \quad (1)$$

where w_0 is the laser spot size at the sample, δ is the modulation amplitude and σ_p is the extinction cross-section of the nano-object. Eqn (1) is strictly only applicable to particles much smaller than the laser spot size,⁵¹ which is fulfilled for the isolated particles in Fig. 1. Given values of $w_0 = 900$ nm and $\delta = 500$ nm, fitting the experimental data to eqn (1) pro-

vides the extinction cross-section of the particle. The accuracy in these measurements is estimated to be 8%, mostly due to the uncertainty in the laser spot size (± 15 nm).

The minimum particle size that can be detected in the SMS measurements is determined by the background noise, which arises from several sources. First, material on the substrate can cause inhomogeneities in the local refractive index, which can scatter the laser beam. An example of this can be seen in Fig. 1(B), where the data recorded at 637 nm shows a feature in the bottom right corner that is stronger than in the corresponding 785 nm image in Fig. 1(A). This is opposite to what we expect based on the absorption spectrum of the dye loaded particles, and is consistent with the feature arising from scattering (the scattering cross-section increases with decreasing wavelength). Noise in the laser source also creates a background signal. This noise can be reduced by increasing the averaging time in the experiments, or by using a balanced detector.³² A third source of noise that can arise in SMS experiments implemented with GSMs is a background signal from clipping the beam.^{51,52} Analysis of our images yields a sensitivity of 800 nm^2 for the experiments on the samples spin coated onto glass coverslips (such as in Fig. 1), and 1000 nm^2 for experiments in cells (see Fig. 2 below). In both cases the major contribution to the noise is from refractive index inhomogeneities in the sample.

Fig. 1(E) shows an image recorded over a wider area ($20 \times 20 \mu\text{m}$) for the croconaine-doped LPNPs where a number of particles can be seen. A histogram of the extinction cross-section per particle determined from several such images is presented in Fig. 1(F). The histogram for this sample is not symmetrical, and reflects the distribution of sizes in the LPNP system (larger particles should, on average, have more dye). A similar non-symmetrical size distribution is present in TEM images of croconaine doped LPNPs (see the ESI†).

For the croconaine-doped LPNPs, the total extinction cross-section can be used to estimate the number of croconaine molecules per particle (assuming that scattering is not significant at 785 nm) by simply dividing by the extinction cross-section for a single croconaine dye.⁴⁸ Croconaine dye in solution has a molar absorptivity of $2.7 \times 10^5 \text{ M}^{-1} \text{ cm}^{-1}$ at the absorption maximum.⁴⁷ This corresponds to an extinction cross-section of 0.10 nm^2 at 785 nm (which is slightly to the blue of the absorption maximum). However, the dye is strongly aggregated when it is incorporated into the LPNPs, which broadens the spectrum.^{53–55} This can be clearly seen in the spectra presented in Fig. 4 below. The assignment that the broadening is due to aggregation was confirmed by adding the LPNPs to DMSO, which released the dye and eliminated the aggregation band. To obtain the extinction cross-section of the aggregated dye, we normalized the absorption spectra by their area, and multiplied the cross-section for the free dye by the ratio of the absorbances for the free dye and dye incorporated into the LPNPs at 785 nm. This yields an extinction cross-section for the LPNP dye of 0.028 nm^2 . The average extinction cross-section for the croconaine-doped particles is $7040 \pm 560 \text{ nm}^2$, with a standard deviation of 39%, which implies that the average number of dye molecules per particle is $250\,000 \pm 20\,000$. Note that this analysis assumes that the degree of dye aggregation is similar for different nanoparticles, and that scattering contributions to the extinction can be neglected (this second assumption is supported by the data in Fig. 1). Determining the average number of dye molecules per particle by conventional measurements is not a trivial problem for this system, because the number of LPNPs is not known.

Cell imaging studies examined the uptake of croconaine-doped LPNPs after incubation for 24 hours with living EMT-6 breast cancer cells. A single layer of fixed cells was imaged on a standard coverslip and Fig. 2 shows SMS images of a single cell containing croconaine-doped LPNPs. Fig. 2(A) and (B) are cell SMS images recorded at 785 nm and 637 nm, respectively, and a bright field image of the cell taken using a CMOS camera is shown in Fig. 2(C). The croconaine-doped LPNPs are clearly observed in the SMS images, but not the bright field image. Note that changing the focus of the microscope does not change the number of particles that appear in the image. This indicates that the particles are located within a fairly narrow range of focal planes in these fixed cell samples. Additional SMS and bright field images of different cells are presented in the ESI.† Fig. 2(D) shows a histogram of the extinction cross-section per particle determined from the data in Fig. 2(A). The total number of dye molecules in the cell was determined by summing up the cross-sections of all the particles and dividing by the cross-section for a single LPNP dye. For the cell in Fig. 2(A) we obtained $N_{\text{dye}} = (55 \pm 4) \times 10^6$.

Fig. 3(A) shows a histogram of the cross-section per particle for the cell experiments, taken from the analysis of 25 different cells (note that the minimum observable cross-section in the cell experiments is $1 \times 10^3 \text{ nm}^2$). The average extinction cross-section per particle is $13\,800 \pm 1100 \text{ nm}^2$ for

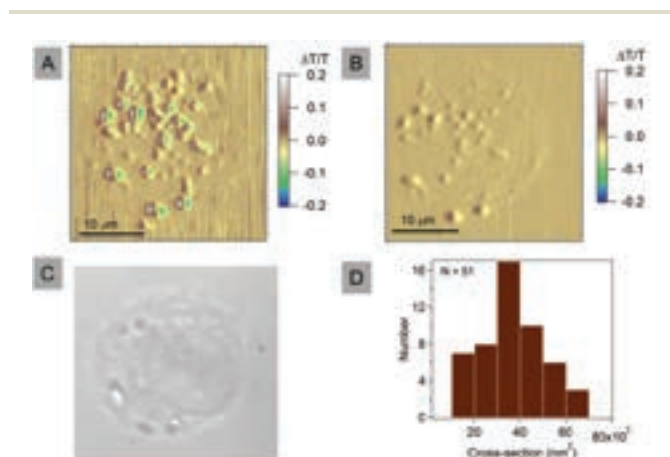


Fig. 2 Wavelength dependent SMS signal images for a single EMT-6 cell. (A) 1f contour plot recorded at 785 nm. (B) 1f contour plot recorded at 637 nm. (C) Bright field image of the cell recorded with a white light source and a CMOS camera. (D) Histogram of the extinction cross-section per particle from the image in (A).

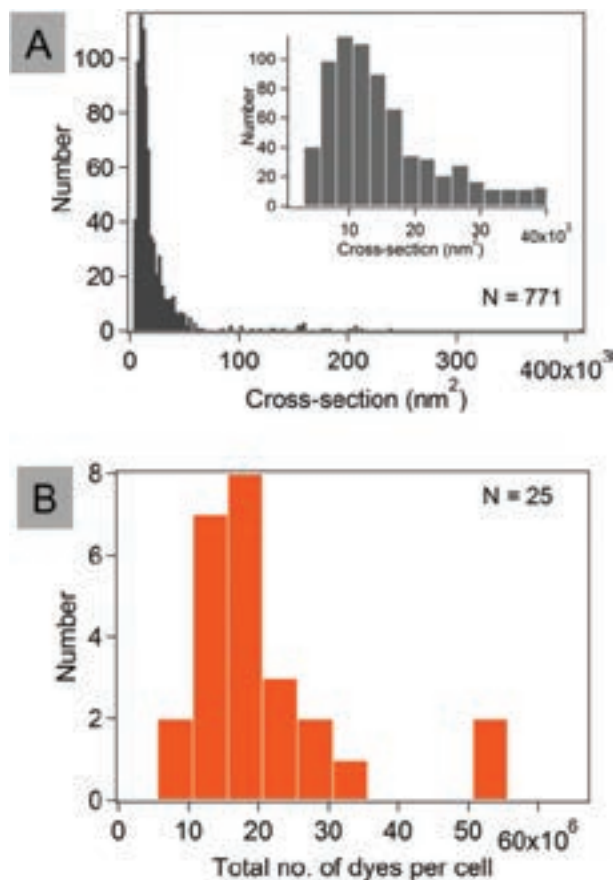


Fig. 3 (A) Histogram of the extinction cross-section per particle for particles incorporated into cells. A total of 771 particles were interrogated in 25 cells. (B) Histogram of the total number of dye molecules per cell, determined from SMS experiments.

the cell experiments, which is significantly larger than that for the particles that were spin coated onto a glass substrate (7040 nm^2). The inset in Fig. 3(A) shows the cross-section histogram on the same x-axis scale as the data in Fig. 1(F). Comparing the two distributions shows that 81% of the particles spin coated onto the coverslip have cross-sections $<10 \times 10^3 \text{ nm}^2$, whereas, for the cell experiments only 45% of the nano-objects detected have cross-sections $<10 \times 10^3 \text{ nm}^2$.

It does not seem likely that there is a change in the average size and/or the amount of dye in the LPNPs when they are incorporated in the cells, or that the cells selectively take up larger particles from the incubating solution. Thus, we attribute the apparent increase in the particle cross-section in the cell experiments to nanoparticle clustering. SMS is a diffraction-limited experiment that cannot differentiate between particles that are closely spaced together. This apparent clustering most likely arises because the LPNPs are concentrated within endosomes, and there are (on average) several LPNPs per endosome (see the ESI†).^{49,50} These observations are not surprising since non-targeted nanoparticles of this size are known to be taken up by non-specific endocytosis.⁵⁶

Fig. 3(B) shows a histogram of the total number of dye molecules per cell, obtained by analyzing the SMS images from all 25 cells. These results show that, under our conditions, an average of $(17 \pm 1) \times 10^6$ dye molecules are incorporated into the cells. This gives an effective intracellular dye concentration of approximately 10^{-4} – 10^{-5} M .⁵⁷ However, the standard deviation of 28% indicates considerable variation between cells. This variability in dye loading has important consequences for photothermal therapy since the cells will be heated to different degrees. The amount of heating is a critical factor that determines the cell death pathway.^{58–61}

There have been several recent reports of organic nanoparticles doped with non-fluorescent near-IR dyes for photothermal therapy.^{36–42} The SMS experiments described here provide a way to quantitatively image these materials, which is important for optimizing conditions for effective nanoparticle targeting. This type of quantification is not possible with fluorescence based measurements, and is only possible in Rayleigh scattering experiments in the sense that scattering allows one to count the number of particles.^{13,62} A drawback of the SMS method is that it is sensitive to refractive index variations in the sample, which limits the detection sensitivity. A possible solution to this is to combine the SMS experiments with PHI and develop a quantitative imaging instrument that is sensitive only to absorption. However, it is likely that most types of nanoparticle delivery optimization experiments do not require high sensitivity, so that the SMS experiments described above will suffice.

Conclusions

SMS has been used to analyze LPNPs doped with near-IR absorbing non-fluorescent croconaine dye molecules. The extinction cross-section for an average croconaine-doped LPNP was determined to be $7040 \pm 560 \text{ nm}^2$, which corresponds to an average number of $250\,000 \pm 20\,000$ croconaine molecules per particle. Images of cancer cells incubated with the croconaine-doped LPNPs provided quantitative information about the number of dye molecules incorporated into the cells, and also showed evidence for particle clustering within endosomes. These results demonstrate that absorption-based microscopy is a promising method for quantitative analysis of dye-doped nanoparticles inside cells.⁴⁶ Knowledge of dye loading and intracellular nanoparticle location should facilitate future studies to optimize the photothermal effect.⁶² There is emerging literature evidence that nanoparticle targeting to specific cell locations such as the mitochondria leads to enhanced cell death.⁶³ SMS imaging should be an effective tool to evaluate the success of LPNP targeting strategies to reach these intracellular targets. Another long-term goal is to develop photothermal therapy procedures that use parameters such as nanoparticle location, laser fluence, and irradiation duration to control the mechanism of cell death which may open new avenues for cancer immunotherapy.⁶⁰

Experimental section

SMS imaging

A schematic of the experimental set up for SMS is shown in Fig. 4(A). The laser source was chosen depending on the absorption spectrum of the system being studied. The available wavelengths were 532 nm (Coherent Verdi V-5 diode pumped solid-state laser), and 637 nm and 785 nm (Coherent OBIS diode laser modules). In all experiments the laser beam was directed to a homebuilt microscope system using a galvo-scanning mirror system (GSMs, Thorlabs, GVS 012). A high NA (Olympus UPlan FLN, 100 \times , 1.2 NA) microscope objective focused the incident beam onto the sample. The transmitted beam was collected using a second high NA microscope objective (Olympus UPlan FLN, 60 \times , 0.9 NA), and the transmitted power was measured by a silicon photodiode (ThorLabs, PDA36A). 4f lens systems were used to project the beam from the GSMs to the back aperture of the focusing objective, and from the back aperture of the collecting objective to the detector. Bright field images of the samples were recorded using a white light source (ThorLabs, OSL1) and a CMOS camera (ThorLabs, DCC1645C). Absorbance spectra of the free croconaine dye in solution, and the dye incorporated into the LPNPs are presented in Fig. 4(B). Corresponding spectra for SRfluor680 dye, and the croconaine/SRfluor680 co-doped LPNPs are presented in the ESI.†

For the SMS experiments the beam position at the sample was modulated using the GSMs.^{51,52} This creates a modulation in transmitted power ΔP when a nano-object is at the focus of the microscope, which is measured by a lock-in amplifier (Stanford Research Instruments, SR830). The total transmitted power P is measured simultaneously using a digital voltmeter (Keithley, 2000 Multimeter). The typical modulation amplitude used in our experiments was 500 nm. The deflection distance for the GSMs was calibrated using a ruled microscope slide (Edmund Optics, 200 LPMM). The accuracy of the SMS measurements was checked by recording data for Au nanoparticles (see the ESI†). The Au nanoparticle size distribution determined by SMS was found to be equivalent to that measured by TEM, implying that the system was properly calibrated. SMS images were obtained by either raster scanning the sample through the laser spot using a piezo-stage (Physik Instrumente), or by scanning the beam over the sample using the GSMs. Typically, a lock-in time constant of 10 ms was used with a 30 ms integration time between steps, and a step size of 0.1 or 0.2 μm . The power impinging on the sample was controlled *via* a variable neutral density filter (ThorLabs, NDC-50C-2M). The spot size in the experiments was measured both by the CMOS camera and by fitting the SMS signal to eqn (1), and was found to be $w_0 = 900$ nm. This value is relatively large considering the NA of the focusing objective, and arises

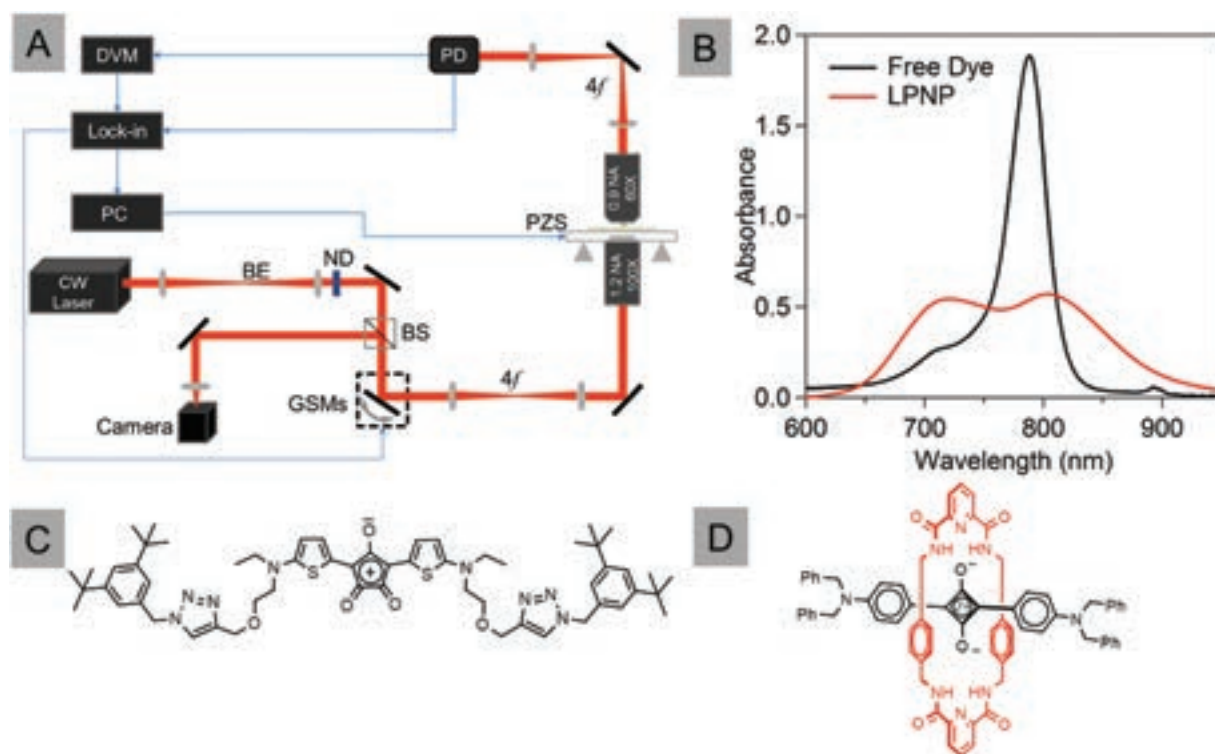


Fig. 4 (A) Schematic of the spatial modulation imaging set up. BE = beam expander, BS = beam splitter, GSMs = Galvo-scanning mirrors, 4f = 4f lens system, ND = neutral density filter, PZS = piezo scanner, PD = photodiode, DVM = digital voltmeter. (B) Absorbance spectrum of the free croconaine dye in solution and of the dye incorporated into the LPNPs. (C) Structure of croconaine dye. (D) Structure of red fluorescent SRfluor680 dye.

because we did not use microscope immersion oil for these experiments.

Nanoparticle preparation

The dye-loaded lipid polymer nanoparticles (LPNPs) were synthesized using an established procedure.^{36,37,40,42} Stock solutions of lecithin and MPEG-DSPE(2000) were each prepared as 1 mg mL⁻¹ in 4 wt% ethanol and stored at 4 °C. The stock solution of PLGA (lactide: glycolide 50:50, ester terminated, MW 7000–17 000) was 2.5 mg mL⁻¹ in acetonitrile. To synthesize the nanoparticles, lecithin stock (12.5 μL) and MPEG-DSPE(2000) stock (200 μL) were added to deionized water (3.7 mL). Solid organic dye (2.0 mg) was dissolved in PLGA stock (400 μL) and slowly added dropwise, such that the final weight ratio was 0.0125:0.2:2:1 lecithin:DSPE-PEG(2000):dye:PLGA. The mixture was sonicated using a probe sonicator for 5 min (20 kHz, 130 W) and the resulting nanoparticle suspension was washed 3 times (4000g, 30 min each time) using an Amicon Ultra-4 centrifugal filter (MWCO 10 kDa) and HEPES buffer (10 mM HEPES, 100 mM NaCl, pH 7.4) to remove remaining organic solvent and dye. The resulting dispersion of dye-doped LPNPs was spin coated onto #1 glass coverslips for the microscopy experiments. The majority of the experiments were performed with croconaine doped LPNPs, and UV-visible absorbance spectra of free croconaine dye, and the dye encapsulated in the LPNPs are presented in Fig. 4(B). Fig. 4(C) and (D) show the chemical structures of the two dyes (croconaine and SRfluor680) used in the experiments.

Cell studies

EMT-6 (ATCC CRL-2755) carcinoma cells were seeded at 70% confluence on 8-chamber covered slides (Lab-Tek) in Waymouth's media (Life Technologies) with 15% FBS, 1% Streptomycin, 1% Penicillin and allowed to adhere for 24 hours at 37 °C and 5% CO₂ over air. The media in each well was replaced with a solution containing 40 μL of LPNP and 960 μL of media (OD₈₀₀ = 0.04). After 24 hours, the media was removed and the cells were washed once with PBS (pH 7.4). The treated cells were detached from the slide with 0.25% trypsin for 5 minutes and transferred to an Eppendorf tube followed by fixation with 10% formalin in PBS for 10 minutes. The cell suspension was centrifuged (3000 rpm, 10 min) to form a pellet, washed twice, and resuspended in 500 μL MilliQ water. A drop of the suspension was allowed to dry for one hour at room temperature on #1 glass coverslips for imaging.

Acknowledgements

This work was supported by the United States National Science Foundation (CHE-1110560), the Office of Naval Research (Award No.: N00014-12-1-1030), the Walther Cancer Foundation Advancing Basic Cancer Research Grant (2013/14) administered by the Harper Cancer Research Institute and the NIH (R01GM059078 and T32GM075762).

References

- 1 K. König, *J. Microsc.*, 2000, **200**, 83–104.
- 2 J. Lippincott-Schwartz, E. Snapp and A. Kenworthy, *Nat. Rev. Mol. Cell Biol.*, 2001, **2**, 444–456.
- 3 E. A. Jares-Erijman and T. M. Jovin, *Nat. Biotechnol.*, 2003, **21**, 1387–1395.
- 4 S. Bolte and F. P. Cordelieres, *J. Microsc.*, 2006, **224**, 213–232.
- 5 S. T. Hess, T. P. K. Girirajan and M. D. Mason, *Biophys. J.*, 2006, **91**, 4258–4272.
- 6 K. I. Willig, R. R. Kellner, R. Medda, B. Hein, S. Jakobs and S. W. Hell, *Nat. Methods*, 2006, **3**, 721–723.
- 7 M. Bates, B. Huang, G. T. Dempsey and X. W. Zhuang, *Science*, 2007, **317**, 1749–1753.
- 8 M. Fernandez-Suarez and A. Y. Ting, *Nat. Rev. Mol. Cell Biol.*, 2008, **9**, 929–943.
- 9 B. Huang, W. Q. Wang, M. Bates and X. W. Zhuang, *Science*, 2008, **319**, 810–813.
- 10 H. Shroff, C. G. Galbraith, J. A. Galbraith and E. Betzig, *Nat. Methods*, 2008, **5**, 417–423.
- 11 C. Eggeling, C. Ringemann, R. Medda, G. Schwarzmann, K. Sandhoff, S. Polyakova, V. N. Belov, B. Hein, C. von Middendorff, A. Schonle and S. W. Hell, *Nature*, 2009, **457**, 1159–1163.
- 12 B. Huang, M. Bates and X. W. Zhuang, *Annu. Rev. Biochem.*, 2009, **78**, 993–1016.
- 13 S. Schultz, D. R. Smith, J. J. Mock and D. A. Schultz, *Proc. Natl. Acad. Sci. U. S. A.*, 2000, **97**, 996–1001.
- 14 J. L. West and N. J. Halas, *Annu. Rev. Biomed. Eng.*, 2003, **5**, 285–292.
- 15 P. K. Jain, X. H. Huang, I. H. El-Sayed and M. A. El-Sayed, *Acc. Chem. Res.*, 2008, **41**, 1578–1586.
- 16 E. Boisselier and D. Astruc, *Chem. Soc. Rev.*, 2009, **38**, 1759–1782.
- 17 G. S. Filonov, K. D. Piatkevich, L. M. Ting, J. H. Zhang, K. Kim and V. V. Verkhusha, *Nat. Biotechnol.*, 2011, **29**, 757–761.
- 18 K. Welsher, S. P. Sherlock and H. J. Dai, *Proc. Natl. Acad. Sci. U. S. A.*, 2011, **108**, 8943–8948.
- 19 V. J. Pansare, S. Hejazi, W. J. Faenza and R. K. Prud'homme, *Chem. Mater.*, 2012, **24**, 812–827.
- 20 K. Rurack and M. Spieles, *Anal. Chem.*, 2011, **83**, 1232–1242.
- 21 C. G. Collins, E. M. Peck, P. J. Kramer and B. D. Smith, *Chem. Sci.*, 2013, **4**, 2557–2563.
- 22 D. Boyer, P. Tamarat, A. Maali, B. Lounis and M. Orrit, *Science*, 2002, **297**, 1160–1163.
- 23 S. Berciaud, L. Cognet, G. A. Blab and B. Lounis, *Phys. Rev. Lett.*, 2004, **93**, 257402.
- 24 L. Cognet, S. Berciaud, D. Lasne and B. Lounis, *Anal. Chem.*, 2008, **80**, 2288–2294.
- 25 A. Gaiduk, M. Yorulmaz, P. V. Ruijgrok and M. Orrit, *Science*, 2010, **330**, 353–356.
- 26 M. Selmke, M. Braun and F. Cichos, *ACS Nano*, 2012, **6**, 2741–2749.

- 27 A. Arbouet, D. Christofilos, N. Del Fatti, F. Vallée, J. R. Huntzinger, L. Arnaud, P. Billaud and M. Broyer, *Phys. Rev. Lett.*, 2004, **93**, 127401.
- 28 A. Crut, P. Maioli, N. Del Fatti and F. Vallee, *Chem. Soc. Rev.*, 2014, **43**, 3921–3956.
- 29 S. Berciaud, L. Cognet, P. Poulin, R. B. Weisman and B. Lounis, *Nano Lett.*, 2007, **7**, 1203–1207.
- 30 P. Zijlstra, P. M. R. Paulo and M. Orrit, *Nat. Nanotechnol.*, 2012, **7**, 379–382.
- 31 J. C. Blancon, M. Paillet, H. N. Tran, X. T. Than, S. A. Guebrou, A. Ayari, A. San Miguel, N. M. Phan, A. A. Zahab, J. L. Sauvajol, N. Del Fatti and F. Vallee, *Nat. Commun.*, 2013, **4**, 2542.
- 32 M. P. McDonald, F. Vietmeyer, D. Aleksasuk and M. Kuno, *Rev. Sci. Instrum.*, 2013, **84**, 113104.
- 33 M. A. van Dijk, A. L. Tchebotareva, M. Orrit, M. Lippitz, S. Berciaud, D. Lasne, L. Cognet and B. Lounis, *Phys. Chem. Chem. Phys.*, 2006, **8**, 3486–3495.
- 34 H. Baida, P. Billaud, S. Marhaba, D. Christofilos, E. Cottancin, A. Crut, J. Lerme, P. Maioli, M. Pellarin, M. Broyer, N. Del Fatti, F. Vallee, A. Sanchez-Iglesias, I. Pastoriza-Santos and L. M. Liz-Marzan, *Nano Lett.*, 2009, **9**, 3463–3469.
- 35 V. Juve, M. Fernanda Cardinal, A. Lombardi, A. Crut, P. Maioli, J. Perez-Juste, L. M. Liz-Marzan, N. Del Fatti and F. Vallee, *Nano Lett.*, 2013, **13**, 2234–2240.
- 36 L. Zhang, J. M. Chan, F. X. Gu, J.-W. Rhee, A. Z. Wang, A. F. Radovic-Moreno, F. Alexis, R. Langer and O. C. Farokhzad, *ACS Nano*, 2008, **2**, 1696–1702.
- 37 R. H. Fang, S. Aryal, C.-M. J. Hu and L. Zhang, *Langmuir*, 2010, **26**, 16958–16962.
- 38 L. Cheng, W. He, H. Gong, C. Wang, Q. Chen, Z. Cheng and Z. Liu, *Adv. Funct. Mater.*, 2013, **23**, 5893–5902.
- 39 S. Mathew, T. Murakami, H. Nakatsuji, H. Okamoto, N. Morone, J. E. Heuser, M. Hashida and H. Imahori, *ACS Nano*, 2013, **7**, 8908–8916.
- 40 M. Zheng, C. Yue, Y. Ma, P. Gong, P. Zhao, C. Zheng, Z. Sheng, P. Zhang, Z. Wang and L. Cai, *ACS Nano*, 2013, **7**, 2056–2067.
- 41 H. Gong, Z. Dong, Y. Liu, S. Yin, L. Cheng, W. Xi, J. Xiang, K. Liu, Y. Li and Z. Liu, *Adv. Funct. Mater.*, 2014, **24**, 6492–6502.
- 42 S. Guha, S. K. Shaw, G. T. Spence, F. M. Roland and B. D. Smith, 2015, submitted.
- 43 D. P. O'Neal, L. R. Hirsch, N. J. Halas, J. D. Payne and J. L. West, *Cancer Lett.*, 2004, **209**, 171–176.
- 44 I. H. El-Sayed, X. H. Huang and M. A. El-Sayed, *Cancer Lett.*, 2006, **239**, 129–135.
- 45 S. E. Skrabalak, J. Chen, L. Au, X. Lu, X. Li and Y. N. Xia, *Adv. Mater.*, 2007, **19**, 3177–3184.
- 46 G. T. Spence, G. V. Hartland and B. D. Smith, *Chem. Sci.*, 2013, **4**, 4240–4244.
- 47 G. T. Spence, S. S. Lo, C. F. Ke, H. Destecroix, A. P. Davis, G. V. Hartland and B. D. Smith, *Chem. – Eur. J.*, 2014, **20**, 12628–12635.
- 48 A. Gaiduk, M. Yorulmaz, E. Ishow and M. Orrit, *Chem-PhysChem*, 2012, **13**, 946–951.
- 49 B. D. Chithrani, A. A. Ghazani and W. C. W. Chan, *Nano Lett.*, 2006, **6**, 662–668.
- 50 A. M. Alkilany and C. J. Murphy, *J. Nanopart. Res.*, 2010, **12**, 2313–2333.
- 51 N. Havard, Z. Li, V. Murthy, S. S. Lo and G. V. Hartland, *J. Chem. Phys.*, 2014, **140**, 074203.
- 52 M. S. Devadas, Z. Li, T. A. Major, S. S. Lo, N. Havard, K. Yu, P. Johns and G. V. Hartland, *Appl. Opt.*, 2013, **52**, 7806–7811.
- 53 I. Martini, G. V. Hartland and P. V. Kamat, *J. Phys. Chem. B*, 1997, **101**, 4826–4830.
- 54 N. C. Maiti, S. Mazumdar and N. Periasamy, *J. Phys. Chem. B*, 1998, **102**, 1528–1538.
- 55 T. Hasobe, S. Fukuzumi and P. V. Kamat, *J. Am. Chem. Soc.*, 2005, **127**, 11884–11885.
- 56 T. A. Kelf, V. K. Sreenivasan, J. Sun, E. J. Kim, E. M. Goldys and A. V. Zvyagin, *Nanotechnology*, 2010, **21**, 285105.
- 57 E. H. Chapman, A. S. Kurec and F. R. Davey, *J. Clin. Pathol.*, 1981, **34**, 1083–1090.
- 58 B. Kang, M. A. Mackey and M. A. El-Sayed, *J. Am. Chem. Soc.*, 2010, **132**, 1517–1519.
- 59 Y. Qiu, Y. Liu, L. M. Wang, L. G. Xu, R. Bai, Y. L. Ji, X. C. Wu, Y. L. Zhao, Y. F. Li and C. Y. Chen, *Biomaterials*, 2010, **31**, 7606–7619.
- 60 M. Pérez-Hernández, P. del Pino, S. G. Mitchell, M. Moros, G. Stepien, B. Pelaz, W. J. Parak, E. M. Gálvez, J. Pardo and J. M. de la Fuente, *ACS Nano*, 2015, **9**, 52–61.
- 61 J. R. Melamed, R. S. Edelman and E. S. Day, *ACS Nano*, 2015, **9**, 6–11.
- 62 Z. Qin and J. C. Bischof, *Chem. Soc. Rev.*, 2012, **41**, 1191–1217.
- 63 L. M. Wang, Y. Liu, W. Li, X. M. Jiang, Y. L. Ji, X. C. Wu, L. G. Xu, Y. Qiu, K. Zhao, T. T. Wei, Y. F. Li, Y. L. Zhao and C. Y. Chen, *Nano Lett.*, 2011, **11**, 772–780.